

Anja K. Stalder^a, Bernd Ilgenstein^a, Natalia Chicherova^{a,b}, Hans Deyhle^a, Felix Beckmann^c,
Bert Müller^a, Simone E. Hieber^a

^aUniversity of Basel, Biomaterials Science Center, Basel, Switzerland

^bUniversity of Basel, Medical Image Analysis Center, Basel, Switzerland

^cHelmholtz-Zentrum Geesthacht, Institute of Materials Research, Geesthacht, Germany

Combined use of micro computed tomography and histology to evaluate the regenerative capacity of bone grafting materials

Pre-clinical animal models are commonly used to evaluate the osteogenic potential of bone grafting materials in-vivo. Based on the histology analysis, the currently commercially available bone grafting materials show comparable results with respect to biocompatibility, incorporation and remodeling. In the present pilot study we introduce a methodology to compare calcium phosphate-based bone grafting materials from world-leading companies in clinical trials and analyze them by means of established histology and synchrotron radiation-based micro computed tomography (SR μ CT). The results indicate that the morphology of the bony structures depends on the selected bone grafting material and that an arbitrarily selected histological slice can lead to misleading conclusions. Complementary μ CT data can become the basis for the identification of a representative slice. The registration of the selected histological slice with its counterpart in the three-dimensional μ CT dataset was performed both visually and automatically with well comparable results. This registration allows for the compilation of a joint histogram to identify anatomical features, which can neither be extracted from histology nor from μ CT data on their own. Accordingly, μ CT will become an integral part of studies on the efficacy of bone augmentation materials and beyond.

Keywords: Registration; Synchrotron radiation-based micro computed tomography; Joint histogram; Tri-calcium phosphates; Hydroxyapatite

1. Introduction

Primary stability and successful osseointegration of dental implants to replace the root of missing teeth depend on local quality and quantity of bone tissue [1]. A sufficient residual bone volume is essential. Alveolar ridge resorption as the result of tooth extraction and pathological defects including periodontal disease, cysts, tumors, and trauma often gives rise to critical bone volume reduction [2–6]. To prevent such bone loss, socket preservation (SP), also termed alveolar ridge preservation (ARP), is performed either by means of autologous bone grafts or bone substitutes. It leads to a statistically significant increase of trabecular

bone with respect to the unassisted socket healing [5, 7]. Besides autologous bone, which has been regarded as the gold standard for decades [8], bone substitute materials play a more and more important role for several reasons. First, recent studies show little effect in fresh extraction sockets, when grafted with autologous bone chips [9]. Second, a larger number of dentists and patients prefer avoiding bone transplants due to the invasiveness of the procedures and the associated morbidity. In these cases bone substitutes offer a vital opportunity to augment the bone defect and subsequently enable the insertion of a dental implant, in general.

Nowadays, a wide variety of bone substitutes are available on the market. Allografts, xenografts, and synthetic materials are applied routinely [10]. Survival rates for dental implants placed into the regenerated sites are reported to be similar to those inserted into sites that do not require bone augmentation [11]. Many in-vivo studies have proven the success rates of the individual, commercially available bone grafting materials. However, there are very few examples in the literature of comparative analyses, i.e. comprehensive and comparative evaluation of the bone substitutes that take advantage of two- and three-dimensional imaging. We hypothesize that the incorporation of micro computed tomography (μ CT) into the well-established, histology-dominated experimental studies on bone augmentation leads to more reliable data and much higher significance of the derived conclusions. To prove our hypothesis, we performed a pilot study considering the bone grafting materials Bio-Oss[®] (Geistlich Pharma AG, Wolhusen, Switzerland), BoneCeramic (Institute Straumann AG, Basel, Switzerland) with an absorbable collagen membrane (Bio-Gide[®] Geistlich Biomaterials, Wolhusen, Switzerland) and easy-graftTM (SUNSTAR Degradable Solutions AG, Schlieren, Switzerland) for socket preservation. The aim of the present communication is not to select the bone grafting material optimized for a certain patient treatment but to present a methodology to compare the materials in clinical trials. The combination of the non-destructive synchrotron radiation-based micro computed tomography (SR μ CT) and corresponding histological sections provides a detailed view of bone morphology and function. First results of the SR μ CT images and histology have been presented [12], but an in depth analysis of the anatomical features is missing due to the lack of a multimodal registration procedure

and joint histograms. As a result a limited number of structures were identified.

The biopsies were extracted for medical reasons and non-destructively gauged by means of synchrotron radiation-based μ CT (SR μ CT) before subsequently being prepared for toluidine blue staining. To exploit the full potential of the combined analysis, the two-dimensional (2D) histology data have to be registered with the three-dimensional (3D) μ CT dataset [13]. The histological images provide a sub-micrometer lateral spatial resolution. The third dimension is typically resolved in the range of 10^{-5} m. The less detailed volumetric tomography data have an isotropic spatial resolution in three directions. Their 2D-3D intermodal registration is performed manually or semi-automatically. Experts visually inspect virtual cuts of the tomography data to identify a satisfactory match with the histology. Interactive registration has been applied for radiofrequency ablation treatment [14], and semi-automatic rigid-body registration methods are available for hard tissues and implants [13, 15]. Fully automatic non-rigid registration [16, 17] remains a challenge because of the many degrees of freedom in the mapping from 2D to 3D and the considerable size of the data sets.

The image registration techniques can be split into two approaches, i. e. landmark-based algorithms [18] and intensity-based methods [19]. While the landmark-based approaches seem attractive for registering large data sets due to their inherent dimensionality reduction ability, matching the landmarks between images of different modalities can be challenging. In intensity-based registration, in contrast, mutual information is used as a well-established similarity measure for multi-modal registration [20].

Despite the existence of 2D-2D and 3D-3D registration algorithms, which are not only available for rigid but also for non-rigid approaches, developments in 2D-3D registration are rarely published [21]. To avoid the alignment from 2D to 3D, various authors [22–25] applied 3D-3D registration techniques to series of 2D stained histological slices and 3D image data sets.

As the 2D histological sections and the 3D CT scans are of different dimensions, an automatic registration process needs to be both scale and translation invariant. Furthermore, rotation and mirroring can occur. Interest points that operate locally and are invariant to the image variations can be considered a basis for 2D-3D registration. Point detectors and descriptors can be provided by the algorithms including Speeded Up Robust Features (SURF) [26] and Scale-Invariant Feature Transform (SIFT) [27].

The inter-modal non-rigid registration enables segmentation of anatomical features of the human tissues, which are undetectable using a single imaging technique [16]. Therefore, we studied which anatomical features of forming bone can be identified by the joint histograms analysis on the basis of the histological and related tomography slices, which can neither be extracted from histology nor from SR μ CT data on its own.

2. Experimental procedures

2.1. Augmentation materials and surgical procedure

Bone specimens for histology and radiological analyses were taken from patients before insertion of dental im-

plants. The written consent of the patients is available. The responsible Swiss authorities ethically approved the procedure.

For Specimen A, the extraction defect was filled with easy-graftTM (SUNSTAR Degradable Solutions AG, Schlieren, Switzerland). Easy-graftTM is a biphasic alloplastic synthetic bone substitute of hydroxyapatite and tri calcium phosphate (TCP). These ceramic granules with a diameter of 600 μ m are fused by a poly lactic acid present as a layer on each granule. The oral surgeon performed the interventions under local anesthesia (Lidocain epinephrine Streuli, Switzerland). The surgery was planned as a two-stage procedure. The first appointment served for socket preservation, while the second intervention was needed for the implantation after healing. The nonsmoking 70-year-old patient was a healthy male with no contraindication for augmentation and implantation. The goal of this kind of intervention was the preservation of the bundle bone area and the avoidance of labial dehiscence defects. After extraction of the right central incisor, the substitute was placed under flapless therapy. Four months later the specimen was extracted with a trephine bur (hollow drill) from the augmented region and the dental implant was inserted with light palatine position. The inner diameter of the trephine bur was 3 mm. The dental implant was inserted under stable regenerated bone conditions (Institute Straumann AG, Basel, Switzerland, bone level implant BL, diameter 4.1 mm, SLActive, length 12 mm). The postoperative treatment and medication included analgesic, irrigation and perioperative antibiotics.

For Specimen B, the bone defect was substituted with Bio-Oss[®] Block (Geistlich Biomaterials, Wolhusen, Switzerland). Bio-Oss[®] is a xenograft that consists of hydroxyapatite. The oral surgeon performed the intervention under local anesthesia (Lidocain epinephrine Streuli, Switzerland). Again, the dentist performed a two-stage surgery. The augmentation patient was a 45-year-old male nonsmoker without contraindication. The therapeutic operative indication for the augmentation was an osteotomy of an ankylosis-ingrown left canine. The access was performed with a horizontal mid-crestal incision and two vertical incisions and the preparation of a lateral muco-periosteal flap. After visualization of the operation area the tooth was removed and the bone substitute was adapted and covered by a collagen membrane (Bio-Gide[®] Geistlich Biomaterials, Wolhusen, Switzerland) according to the guided bone regeneration technique (GBR). The intervention was completed with an extended periosteal incision and wound closure with non-absorbable sutures. Eleven months later, we used a trephine bur with an inner diameter of 2 mm to harvest Specimen B, before the implant was inserted. The implant (Institute Straumann AG, Basel, Switzerland, bone level implant BL, diameter 4.1 mm, SLActive, length 12 mm) was inserted in the planned position within the bone augmentation area and post-operatively treated as described for Specimen A.

For Specimen C, a vertical bone defect in the region of a right first molar was augmented with BoneCeramic[®] (Institute Straumann AG, Basel, Switzerland). The synthetic material is a biphasic alloplastic bone graft. It consists of a mixture of hydroxyapatite and tri calcium phosphate with grain diameters of 400 to 700 μ m and a porosity of 90 %. The oral surgeon performed the two-stage intervention un-

der local anesthesia (Lidocain epinephrine Streuli, Switzerland). The intervention was necessary due to an extended vertical bone defect after the extraction of a right first molar. The 46-year-old patient was a healthy nonsmoker. The indication for a vertical augmentation was a limited bone height to the maxillary sinus. After a horizontal midcrestal and two vertical incisions a muco-periosteal flap was prepared and granulation tissue removed. A new alveolar crest was built up by the BoneCeramic substitute. The augmented alveolar crest was covered by a collagen membrane (Bio-Gide[®] Geistlich Biomaterials, Wolhusen, Switzerland). After five months of bone healing of the vertical defect Specimen C was harvested with a 3 mm diameter trephine bur at the planned implant position. The implant (Institute Straumann AG, Basel, Switzerland, standard implant WN, diameter 4.8 mm, SLActive, length 8 mm) was inserted under stable conditions. The post-operative treatment and medication were as described above.

Figure 1 shows an example of the bone grafting procedure performed with easy-graftTM. The non-restorable tooth indicated signs of inflammation in its periodontal soft tis-

sue. If these cases are not treated, one observes bone resorption. Therefore, the tooth was graded as hopeless with indication for extraction. For aesthetic and functional reasons the tooth needed a replacement that included a dental implant. In this case, the implantation was planned as described for Specimen A. After extraction and augmentation with easy-graftTM the alveolar ridge presented in a stabilized condition after a period of six months bone healing. The harvesting of the biopsy with trephine bur was done in the session for implantation. The dental implant was inserted at the position, from where the biopsy was taken. The biopsy was further processed for SR μ CT measurements and histology. Figure 1h shows the reconstructed site with the artificial crown.

2.2. SR μ CT data acquisition

To reveal the 3D morphology of the three specimens, synchrotron radiation-based micro computed tomography (SR μ CT) measurements were carried out at the beamline W2 at HASYLAB/DESY, Hamburg, Germany in conven-

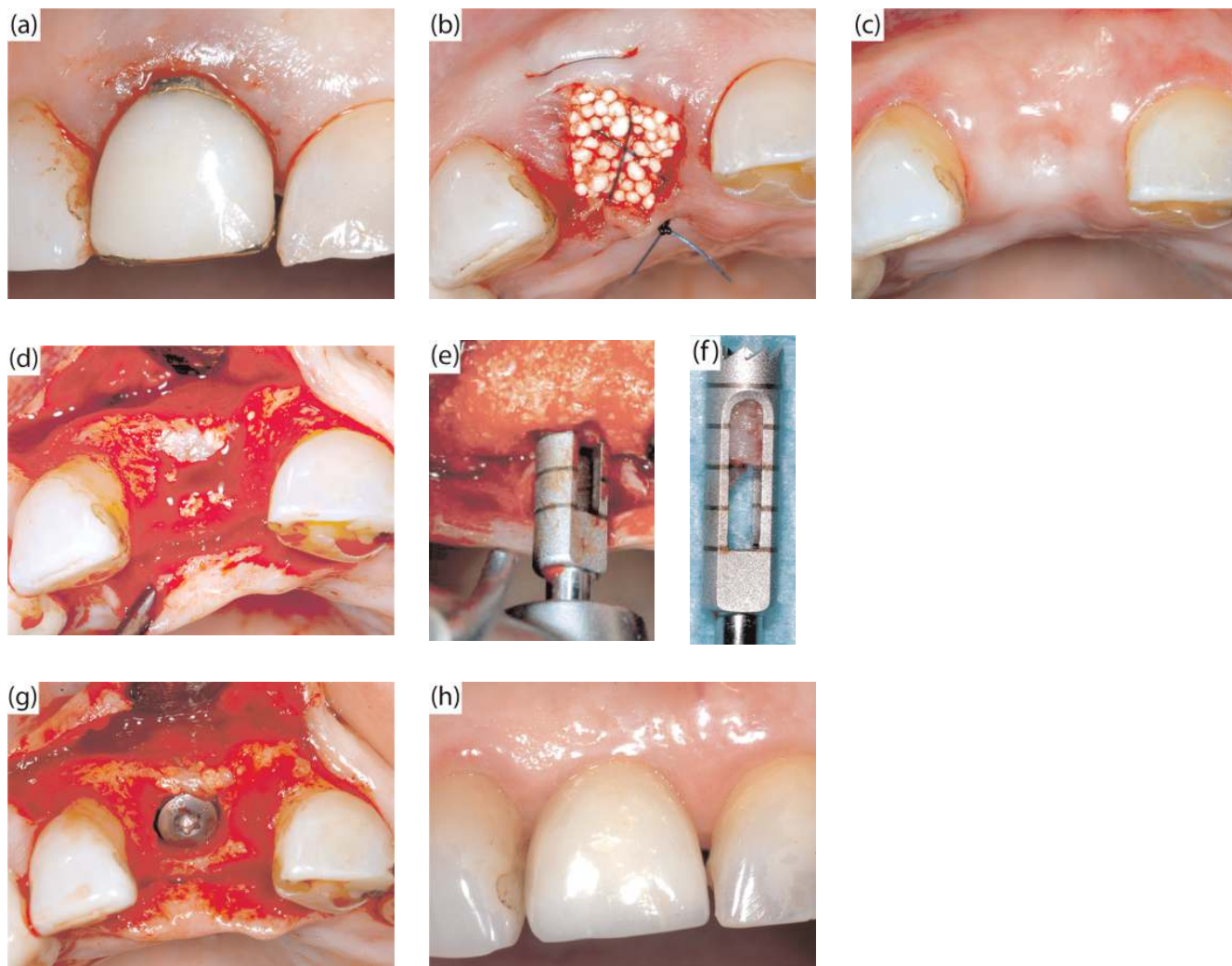


Fig. 1. The common surgical procedure of bone augmentation and of tooth reconstruction includes several visits to the dental office. (a) Marginal signs of gum infection at the no longer prosthetically restorable tooth, (b) alveolus augmentation with easy-graftTM, (c) stabilized alveolar ridge after four month bone healing, (d) intraoperative view to the preserved alveolar ridge before implantation, (e) harvesting the biopsy with trephine bur, (f) trephine bur with the biopsy, (g) inserted dental implant exactly at the site of harvested bone biopsy, (h) successful reconstruction.

tional absorption contrast mode [28]. The HZG Research Center, Geesthacht, Germany operated the beamline and the SR μ CT system. The detector consisted of 3056 \times 3056 pixels, which were binned by a factor of two before reconstruction. For the tomography data acquisition of Specimen A the photon energy was set to 25 keV and the non-binned pixel size to $(2.17 \mu\text{m})^2$, which resulted in a spatial resolution of $4.37 \mu\text{m}$ that we derived from the 10% value of the modulation transfer function of a highly X-ray-absorbing metal edge [29]. For Specimen B and Specimen C the photon energy also corresponded to 25 keV but the pixel size was slightly smaller at $(2.16 \mu\text{m})^2$ given a spatial resolution of $4.14 \mu\text{m}$. The tomography data were obtained from a set of 721 equiangular radiographs along 180° by means of the standard filtered back-projection reconstruction algorithm [30]. To obtain the 3D representation of the entire specimens, tomograms at different vertical positions were combined with voxel precision [17]. The commercially available software VGStudio MAX 2.0 (Volume Graphics, Heidelberg, Germany) served to visualize the tomography data.

2.3. Histology

After the SR μ CT analysis the three biopsies were further processed for histology. The embedded specimens were placed in customized polytetrafluoroethylene molds and re-embedded with a methyl methacrylate solution consisting of methacrylate-methyl ester (Sigma-Aldrich Chemie GmbH, Buchs, Switzerland); dibutyl phthalate (Merck-Schuchardt OHG, Hohenbrunn, Germany) and Perkadox (Dr. Grogg Chemie AG, Stetten, Switzerland) in a ratio of 89.5 : 10 : 0.5. To ensure an almost vertical position of the cylindrically shaped specimens during the polymerization process, the cylinders were held in place using cured methacrylate blocks prepared earlier from the same solution. After embedding the specimens were stored and dried at room temperature. A diamond saw (Leica 1 SP 1600, Leica Instruments GmbH, Nussloch, Germany) served for cutting thick circularly shaped sections of the biopsies.

The sections were glued (Cementit CA 12, Merz+Benteli AG, Niederwangen, Switzerland) on opal acrylic slides (Perspex GS Acrylglas Opal 1013, Wachendorf AG, Basel, Switzerland), wrapped in aluminum foil and pressed overnight under a metal block of 1 kg weight.

Further thinning to $300 \mu\text{m}$ was achieved through grinding (EXCAT CS400, EXACT Apparatebau, Norderstedt, Germany) and treatment with sandpaper (grit size 1200, Struers GmbH, Birmensdorf, Switzerland).

Subsequently, the surfaces were polished on a Struers Planopol-V (Struers GmbH, Birmensdorf, Switzerland) with sandpaper (grit size 4000, Struers GmbH, Birmensdorf, Switzerland). The polished sections were etched with formic acid (formic acid, 0.7%, Sigma Aldrich, Buchs, Switzerland) for two minutes, cleared and etched for another two minutes, rinsed with water and later surface stained with toluidine blue (1% stock solution in 0.1 M phosphate buffer pH 8.0, Sigma Aldrich, Buchs, Switzerland) for ten minutes. The sections were digitally recorded with a microscope (Leica M420, Camera DFC 320, Leica Microsystems, Heerbrugg, Switzerland, magnification $1.0 \times 18.6 - 22.3$) using the software Image Manager 1000 (Leica Microsystems, Heerbrugg, Switzerland) [12].

2.4. 2D-3D registration

The combination of histological images and μ CT data for the bone assessment requires the multi-modal mapping of 2D slices on 3D data sets. Due to the complexity of 2D-3D registration the present study followed two approaches, namely a visual inspection by an expert and an automatic search in a restricted part of the tomography data.

The cutting directions of the histology were identified manually by means of the visualization software VG Studio Max 2.0 (Volume Graphics, Heidelberg, Germany). The positions of the histological slices in the volume data set and the rotation angle were determined by manual and automatic searches. The automatic 2D-3D registration was developed on the basis of the scale-invariant feature transform (SIFT) approach [27]. The SIFT algorithm extracts distinctive image features that are invariant to scale and rotation and matches them with a high degree of reliability. The algorithm was applied to the histological images converted to grayscale and to slices of the CT data sets in the histological cutting directions. The resulting matching landmarks showed a high degree of similarity. The five μ CT slices with the largest number of matching points per histological cut were examined visually to identify the best match.

A joint histogram is a two-dimensional matrix, where the entries represent the number of pixels within the physical quantities represented by means of gray value intervals of two images preferably showing the same object. The number of intervals for the histological image of size 1896×1896 is 306 according to the Rice rule, which suggests twice the cube root of the number of observations [31]. For computational reasons we chose the closest power of two, namely 256, and distributed the intervals uniformly.

The preparation of joint histograms included the non-rigid registration of the selected 2D images. It was performed by a demon algorithm that is based on the maximization of mutual information and implemented by Kroon et al. [32]. The data processing was performed in Matlab 8 R2012b (Simulink, The MathWorks, Inc., USA) including the SIFT toolbox provided by Lowe [27].

2.5. Further analysis of bone formation

The cylindrically shaped biopsies were cut perpendicular to their long axis resulting in a reasonable number of circular sections. A rectangular biopsy cut parallel to the long axis could yield more extensive information regarding bone formation and resorption of the grafting material throughout the entire biopsy, but cannot be obtained simultaneously. Using the non-destructively obtained tomography data the scientists can decide which histological cuts belong to the most promising ones.

Histology allows the identification of augmentation material as well as bone in its varying developmental stages. Newly formed bone, non-resorbed augmentation material, soft tissue and not yet mineralized portion of the bone (osteoid) can be distinguished. Comparison of histology with the tomography data enables the correlation of the X-ray absorption values with the tissue types present. After the identification of the X-ray absorption ranges for bone, augmentation material and soft tissue/embedding the volume of the material phases can be evaluated quantitatively using the histogram of the data [33]. The material phases are re-

presented by Gaussian functions fitted to the histogram (see Fig. 2). The Gaussian fits were calculated by applying the Levenberg–Marquardt algorithm in proFit software 6.2.11 (Quantum Soft, Uetikon am See, Switzerland).

3. Results

3.1. Clinical results

Bone augmentation procedures were successfully performed for the three patients. There were no reported complications. After the healing period, sufficient bone was offered to place the implant as indicated in Fig. 1. Both insertion of the dental screw implant and the placement of the artificial crowns were successfully performed. No complications after these interventions were reported.

3.2. Histogram analysis

After cropping the biopsy from the μ CT data set, one can analyze the components on the basis of the histogram. Figure 2 displays the histogram of the 3D μ CT data for Specimen A on a logarithmic scale. The three main peaks can be easily identified as embedding material and soft tissues (light gray), mineralized bone (dark gray) and augmentation material (black). There is another peak between embedding and bone, which is difficult to fit by means of a Gaussian and which is associated with newly formed bone with a variety of mineralization stages. The peak between bone and augmentation material can be related to the degrading augmentation material. The integral frequencies as represented in color indicate the volume fractions of the harvested biopsy. In Specimen A we found 1.3% easy-graftTM, 34.1% bone, and 64.6% embedding material, which also includes the soft tissue components. Using thresholding in the visualization tool VG studio, the following volume fractions were identified: Specimen B included 57% soft tissue and embedding, 14.2% bone, 25.7% Bio-Oss[®] (including bone in Bio-Oss[®]), Specimen C contained 45.5% soft tissue and embedding, 4.7% BoneCeramic[®] and 48.9% bone.

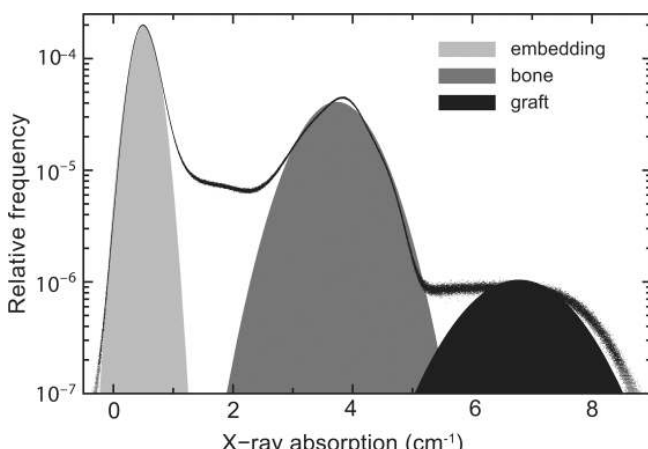


Fig. 2. The Gaussian fits to the 3D histogram of Specimen A reveal the volume fractions of embedding/soft tissues (65%), bone (34%) and augmentation material (1%).

3.3. 2D-3D registration

Figures 3 to 5 compare the histological slices with the registration results of the manual and automatic search for Specimens A to C. Both approaches identify μ CT slices that show close similarities with the corresponding histological slices. There are only a few exceptions for the algorithmic approach. More than 75% of the μ CT slices determined by manual and automatic registration are less than 0.1 mm apart. The manual search leads to generally better results than the current approach of automatic searching. The algorithmic approach fails for the Specimen B at position 1.5 and 2.2 mm. The visual inspection is, however, a time-consuming procedure, which needs validation. The manual registration required approximately 8 h per slice while the mean computational time for the automatic search on a personal computer was approximately 10 times faster (Intel[®] Core[™] i7-2600 3.4 GHz, 16 GB RAM). The characteristic anatomical structures of the specimens including mature bone and augmentation material are displayed well in both histology and tomography. The three specimens feature conspicuous differences in the morphology. In the histological slices, the following tissue types can be identified and distinguished: fully mineralized bone, newly formed bone, non-resorbed augmentation material, soft tissue/embedding material and not yet mineralized bone (osteoids).

3.4. Correlation between the μ CT slices and the entire biopsy

To determine how far the selected histological slices are representative for the entire biopsy, one can analyze the cross-correlation between the individual histograms of μ CT slices and their corresponding slice from the 3D data. For Specimen A and Specimen B the correlations are larger than 94%, whereas they vary between 70% and 98% for Specimen C (see Fig. 6). The CT data set of Specimen A features reconstruction artifacts at the slice positions 2 and 4 mm leading to drops in the correlation profile. The neglect of affected slices in the histogram evaluation leads to a change in the cross-correlation of only 0.1%. Regarding the histograms, the histological slices close to the positions 0.1, 2.8 and 3.6 mm are the most representative ones for Specimen A, the slices at 1.3 and 3 mm for Specimen B and the slices at 1.2 and 1.6 mm for Specimen C.

Figure 7 shows the histogram of the Specimen C compared to CT slices at the positions 1.6 and 1.8 mm. While the slice at position 1.6 mm has a high cross-correlation of 96%, the slice at 1.8 mm has a relatively low one of 80%. The difference in correlation can be recognized well in the histogram matching.

3.5. Combination of micro computed tomography and histology

Figure 8 shows the X-ray absorption histogram of Specimen B and the histograms of the converted histological sections. The inverted red and blue color channels of the histology data are plotted and manually adapted such that the main peaks coincide with the ones of the μ CT histogram. The peak located close to an absorption value of 1 cm^{-1} represents the soft tissue/embedding material, the one close to 3.8 cm^{-1} corresponds to the newly formed bone, and the

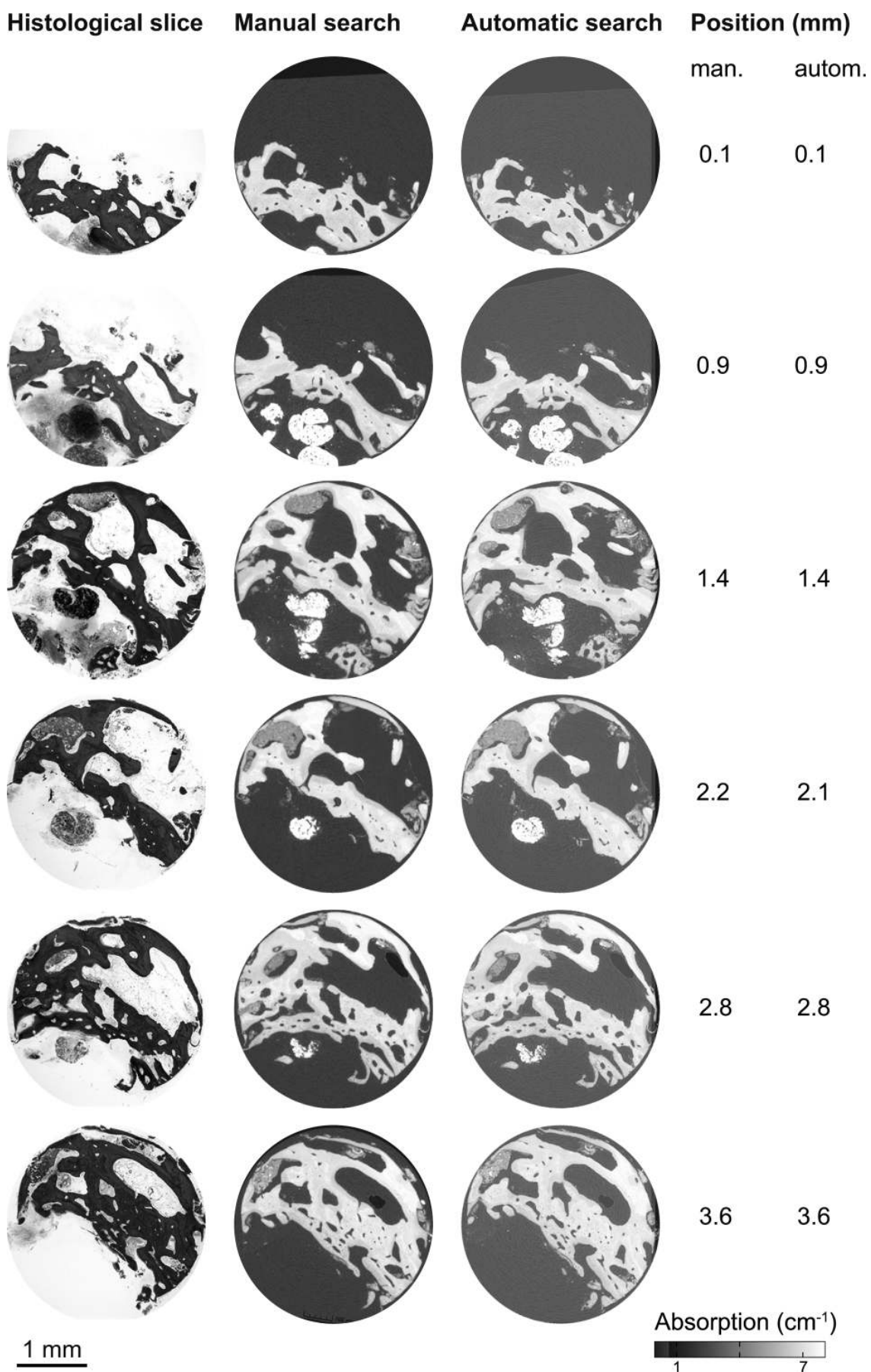


Fig. 3. The comparison of selected histological slices (left) with manually (middle) and automatically (right) registered μ CT slices for Specimen A (easy-graftTM).

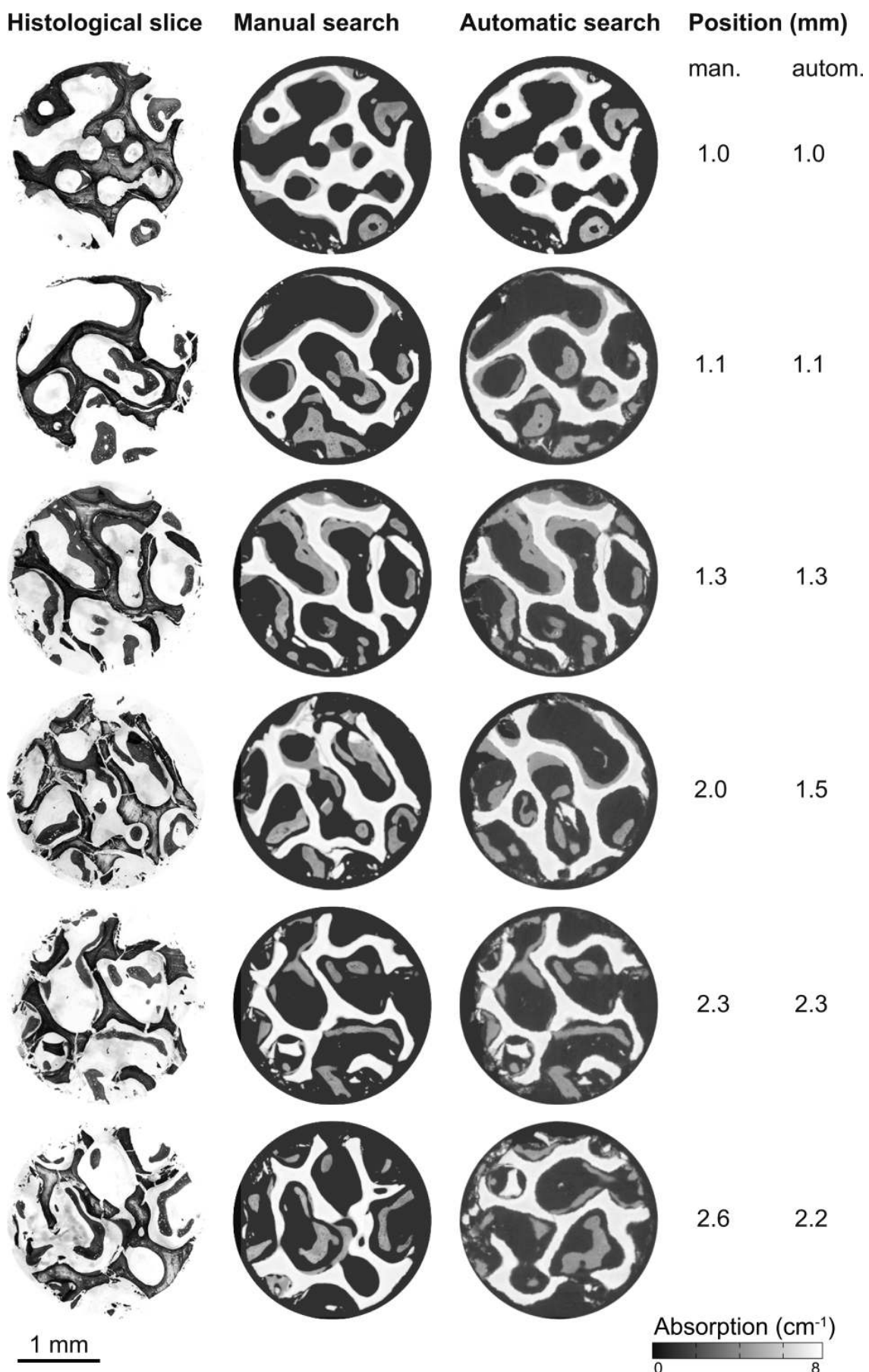


Fig. 4. The comparison of selected histological slices (left) with manually (middle) and automatically (right) registered μ CT slices for Specimen B (Bio-Oss[®]).

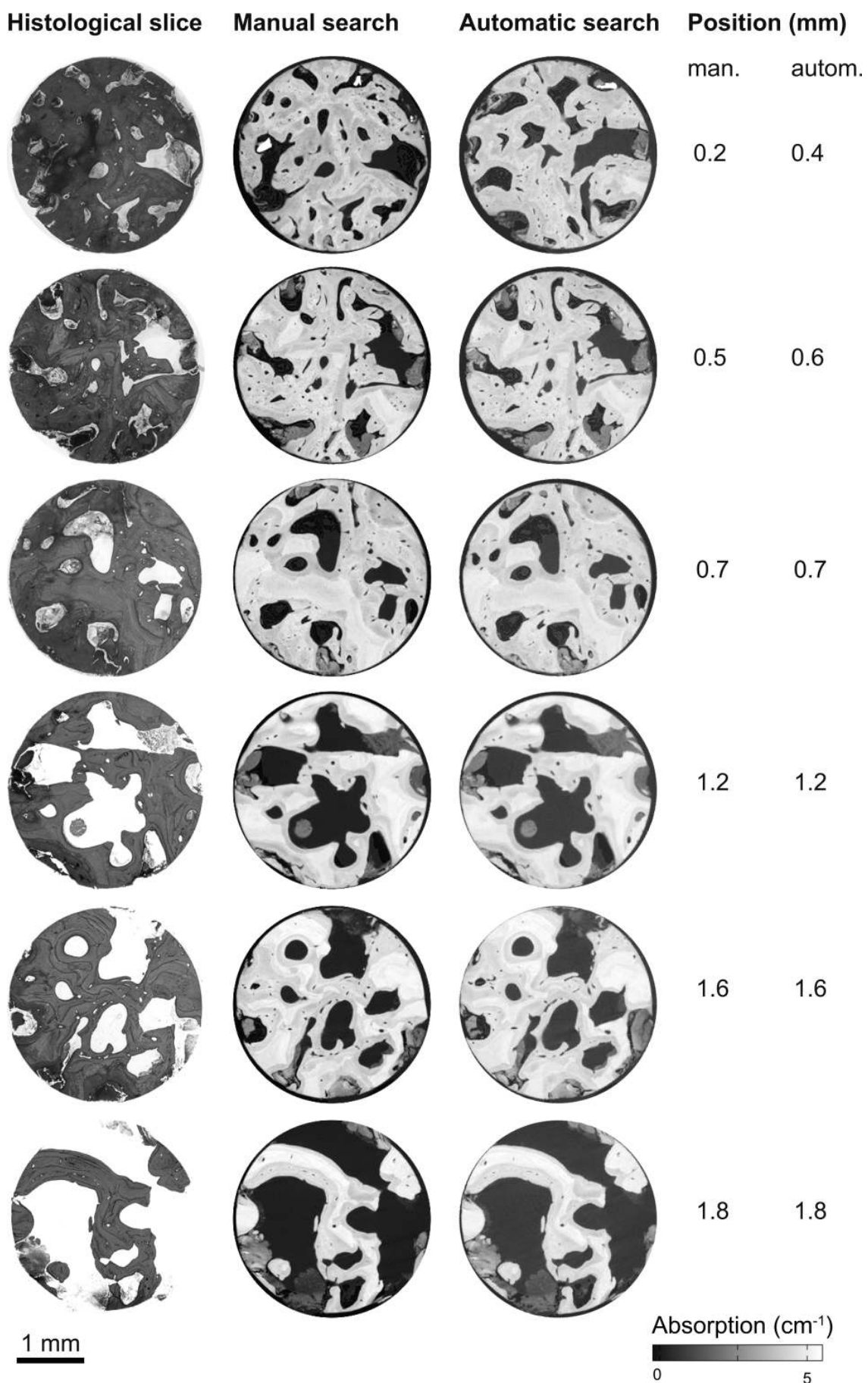


Fig. 5. The comparison of selected histological slices (left) with manually (middle) and automatically (right) registered μ CT slices for Specimen C (BoneCeramic[®]).

one at 7.5 cm^{-1} to the augmentation material. The μ CT histogram exhibits the three peaks in a clear manner such that the materials can be separated by thresholding based on the local X-ray absorption values. Since the bone augmentation material is colored in dark purple the red channel of the histological image features a peak in the histogram that coincides with the one of the μ CT at an absorption value

of 7.5 cm^{-1} . The blue channel reveals the newly formed bone in a similar manner. The histogram of the histological slice shows only two peaks after the conversion from color into grayscale preventing the distinction of three materials.

The joint histogram, which is represented for Specimen C at the position 1.2 mm in Fig. 9, combines the information from the histological slice (histogram on the left) with the corresponding μ CT slice (histogram on the top). The combination allows for the identification of newly forming bone (blue) and bone augmentation material (red) that cannot be extracted based on the histogram of the histology or the tomography slice alone. The gradient from dark to bright red denotes the degradation of the augmentation material. The green region indicates the joint histogram range of soft tissue (granulation tissue) and mineralizing bone matrix. The corresponding grayscale slices in panels A and B are colored as represented in the joint histogram.

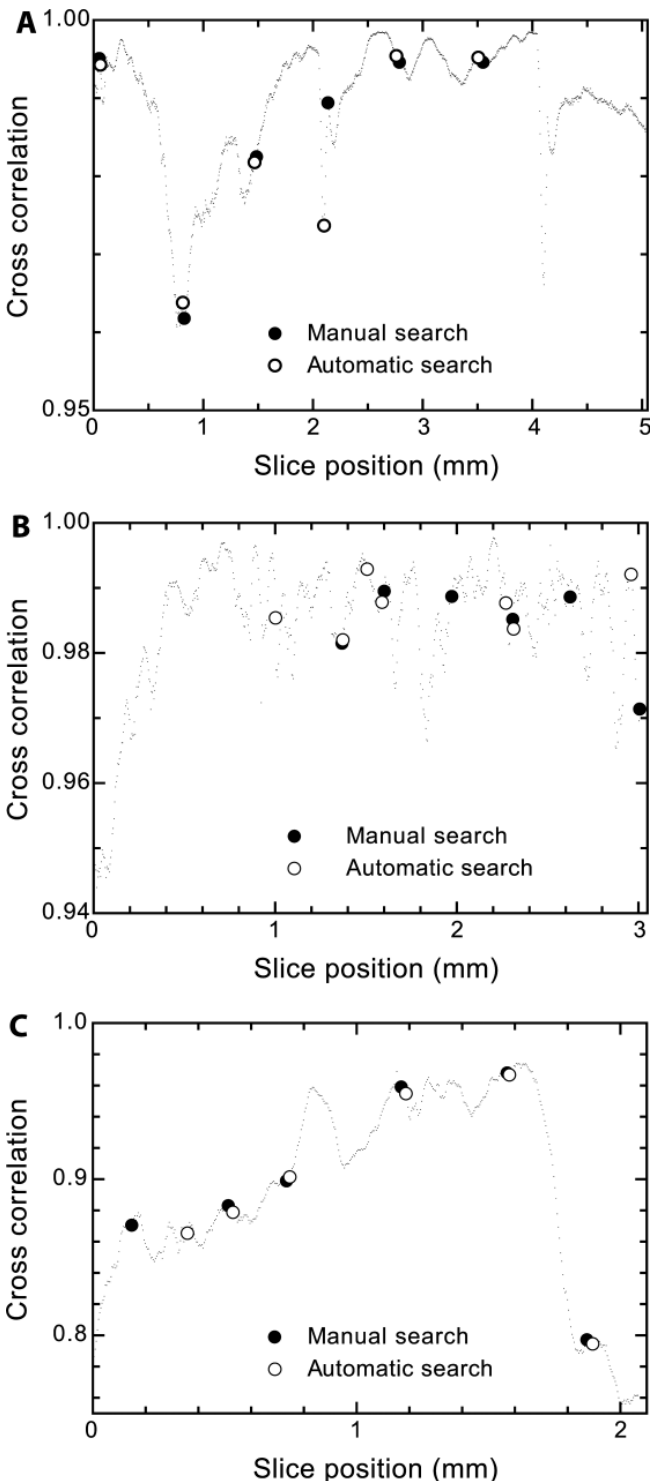


Fig. 6. The cross-correlations of the CT slices with respect to the entire 3D data set of the cylindrically shaped Specimen A (top), Specimen B (middle) and Specimen C (bottom) together with the manually and automatically found slice positions.

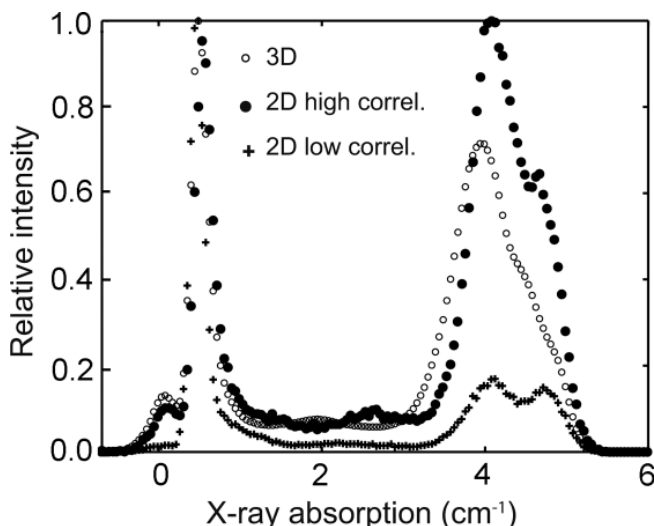


Fig. 7. The histograms of the μ CT slices determined for the histological cuts at position 1.6 mm (high cross-correlation) and 1.8 mm (low cross-correlation) are compared to the 3D histogram of Specimen C.

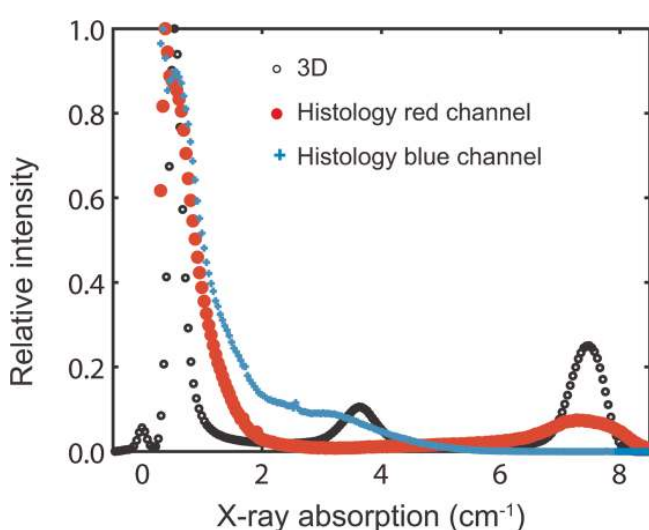


Fig. 8. The histograms of the histological slice (red and blue channel) are compared to the 3D histogram from the SR μ CT data of Specimen B.

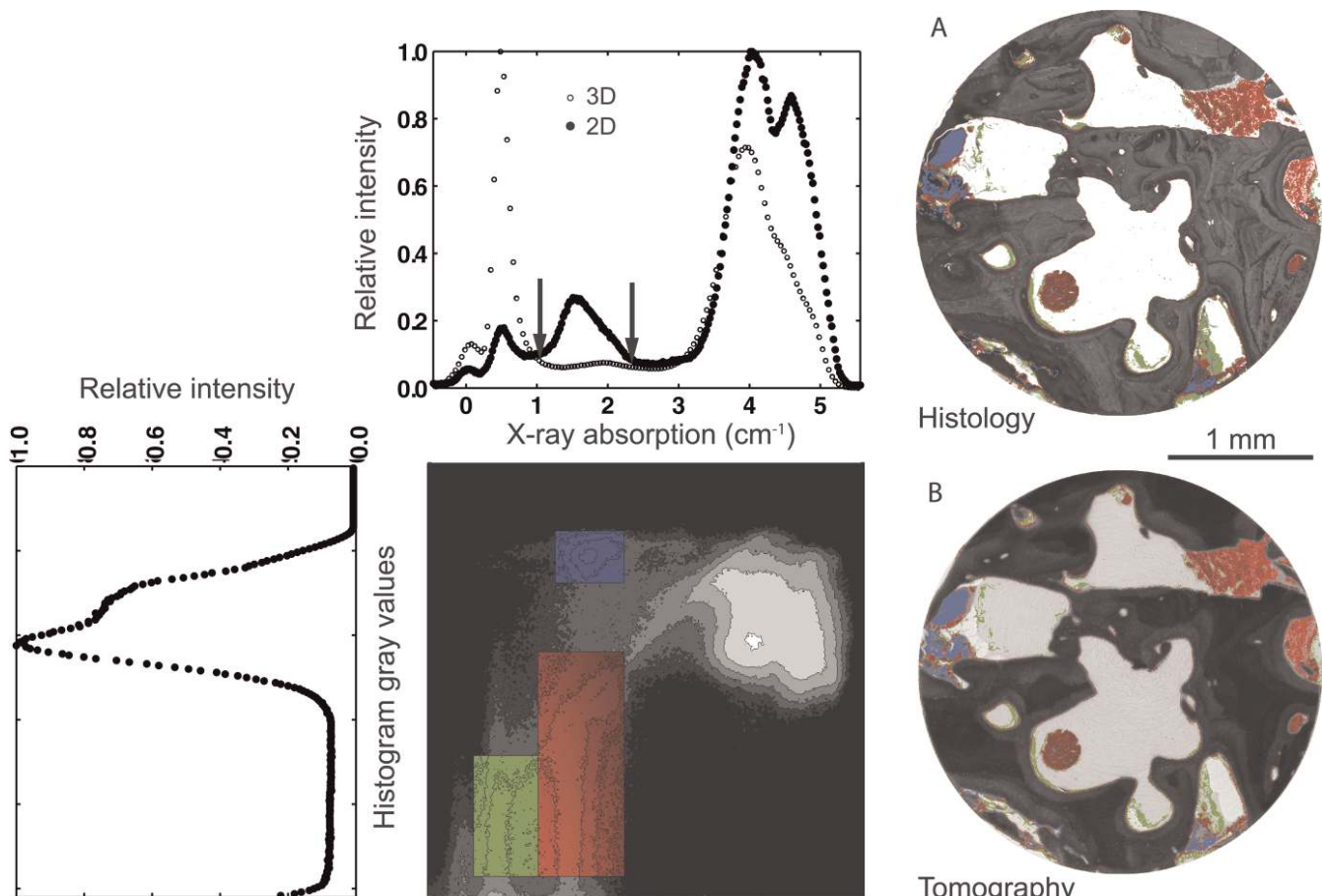


Fig. 9. The joint histogram of histology and SR μ CT slice (Specimen C) allows the segmentation of the partially degraded augmentation material (red), the early formed bone (blue) and the soft tissue (granulation matrix)/mineralizing bone matrix (green). The gradient from dark to bright red represents the degradation of the augmentation material.

The comparison with the 3D histogram shows that the selected μ CT slice includes a larger amount of newly formed bone/augmentation material and a smaller one of soft tissue/embedding material than the average. Nevertheless the histograms have a correlation of 96 %.

4. Discussion

Frequently, bone tissue must be supported or reinforced by augmentation materials before dental implants can be inserted because of bone loss after extraction therapy, pathologic bone defects or trauma. Bone substitution with calcium phosphate phases and xenografts has become more and more common as the alternative procedure to reconstruction with autologous human bone [34–37].

So far, bone resorption cannot be totally prevented by alveolar ridge preservation. Particularly, the outcome of socket preservation is insufficiently discussed in the literature [5, 38]. There is agreement that the use of a hollow drill is a feasible mean to obtain a biopsy from the site of implantation [12, 36, 37, 39–41]. The biopsy can contain many components: hard and soft tissues as well as augmentation material. Therefore, the preparation of histology slices is challenging and the augmentation material usually quarries out during sectioning, see for example Refs. [12, 42]. Hence, the well-established histological evaluation of

bony tissues should be complemented by non-destructive techniques such as μ CT, which have been used for decades to evaluate bone specimens without augmentation material [12, 43]. In a more recent study, SR μ CT is applied to biopsy specimens, which suitably shows the micro-architecture of the bone regeneration pattern and the spatial organization of hard tissue structures [40].

Numerous clinical studies [37, 41] rely on only a few or even one histological slice per specimen. As, for example, demonstrated for titanium implants [44, 45] the choice of slice can massively influence the result of the study. Here, we have introduced an approach to select a representative slice analyzing the cross-correlation of the circularly shaped μ CT slices with the entire cylindrically shaped biopsy volume. This knowledge can guide scientists and technicians to prepare a histological slice that is representative for the biopsy. In the present pilot study, the biopsies were cut perpendicularly to their long axis resulting in a relatively large number of cross-sections. The sections show the characteristic structures at selected heights. Whereas longitudinal sections yield more extensive information regarding bone formation and resorption of the grafting material throughout the entire biopsy, the cutting direction chosen in present study is suitable for the identification of the most representative structures. The cross-correlation can be as low as 70 %, cp. Figures 6 and 7. Selecting the region

for histological sectioning on the basis of the information given in Fig. 6, increases the cross-correlation to more than 99 % for Specimens A and B and to above 97 % for Specimen C. One can even optimize the choice by considering the environment of the dedicated slice, as the precision for the histological sectioning is limited. Thus, the peaks in the cross-correlation curves should be as broad as possible.

It should be noted that, contrary to current opinion, μ CT is performed relatively fast and easily [46]. The application of the nondestructive technique allows for a direct measurement of the bone volume and an easy quantification of bone-related parameters, but has only recently revealed individual cells in special cases [47, 48]. The technique is complementary to histology, which allows the visualization of various tissue types and cellular structures, but is destructive, labor intensive, and time consuming [46]. Particularly, SR μ CT is a valuable tool for the evaluation of bone quality after augmentation with bone substitutes [49]. Compared to conventional laboratory systems, SR μ CT with monochromatic radiation provides not only improved density resolution but also directly gives local X-ray absorption values without calibration procedures to quantify the bone density and the degree of mineralization. Bone tissues with various degrees of mineralization, which depend on healing time, can be characterized using their local X-ray absorption values, as demonstrated in Fig. 8. Because the bone volume could not be measured before the treatment and since the amount and the location of grafting material can only be determined with restricted precision using the in-vivo imaging techniques, a quantification of biodegradation/resorption becomes questionable. Nevertheless, bone remodeling, which includes significant osteoclast activity, is present. A study of the degradation kinetics, however, is expensive, as the biopsy can only be harvested at a pre-defined time point and therefore it only provides a snapshot of the entire remodeling process. Unfortunately, the dose in SR μ CT is so high that in-vivo measurements are not feasible. Another limitation of SR μ CT is its availability restricting the number of extended studies on bone, cp. [40, 50]. The limited number of specimens in the present study does not allow a clinically relevant statement, but rather the development of an evaluation methodology for bone augmentation materials based on SR μ CT and histology. The embedding of bone biopsies into polymers is very convenient and permits suitable storage until beamtime is available. The discrimination of the soft tissue components from the embedding material, however, is usually impossible. Bernhardt et al. [45] showed that the absorption histograms entail one common peak for PMMA, soft tissues and low mineralized bone.

Previous studies showed that two of the bone grafting materials (Bio-Oss[®], BoneCeramic[®]) led to similar clinical and radiological results for bone augmentation [51, 52] and similar histological appearance [36, 37]. The present study reveals morphological differences in the structure of the biopsies. Reasons may be the variations in the healing periods among the different specimens and in the choice of the grafting regions.

The histology facilitates obtaining information regarding cell and tissue function by, for example, using immunohistochemical analysis or enzyme histochemistry. In μ CT, there are only a very few examples, where functional information can be gained, see for example [53].

The complementarity of histology and μ CT is obvious, but their combination might yield even deeper insights by the use of joint histograms as recently demonstrated in the multimodal imaging of the human cerebellum [16]. A joint histogram of the histology and the related SR μ CT slice, however, is a more challenging task, as the μ CT slice has to be found within the dataset of GB size. The registration of 2D with 3D data is usually performed on the basis of visual inspection by comparing the histological slice with more or less arbitrarily chosen virtual cuts of the 3D data. The result of the manual search may depend on the expert. In many cases several experts have to examine the data before a reasonable conclusion can be drawn. Automatic or semiautomatic searches will, therefore, reduce the efforts to identify the correspondence. So far, these approaches rely on rigid or affine registration and the soft tissue deformation in the range of 10 % [54, 55] cannot be corrected in an appropriate manner. To this end, we consider the registration presented in Fig. 9 as a notable achievement. This achievement has to be valued even higher, since the biopsy specimens in our pilot study were re-embedded for histological sectioning. As a consequence, the axes of the CT data were not parallel to the axes of the histological sections. Thus, we re-sampled the SR μ CT data to align them to the histological slices by tilting the data according to manually selected rotation angles. We had to take into consideration that the slices were not perfectly aligned between the set of histological slices but exhibited deviations because of the preparation procedure, which included sawing and grinding. The histological sections may even be curved. As a consequence the results have to be viewed with caution. For example, the red-colored margin of the blue-colored feature in Fig. 9 could be an artifact.

The selected joint histogram of the present communication clearly demonstrates that the combination of histology with the registered μ CT slice enables us to identify anatomical features covered in μ CT and histology. In particular, the early stages of bone formation colored in blue belong to the prominent examples. In the μ CT-data, the partially degraded bone augmentation material (easy-graftTM) shown in red overlaps the preliminary phase of bone. In the histology, the preliminary phase of bone is part of the shoulder from the dominating bone peak. Therefore, the combination of the two techniques provides anatomical features not extractable by one of the techniques alone. The 2D information, as represented in the tomography slice of Fig. 9, can then be extrapolated to the 3D tissue structure by analyzing various sections of the same sample [49] or applying region-growing software [56].

5. Conclusions

The combination of SR μ CT and selected histological sections provides a detailed quantitative view of bone morphology and maturation. The combination of the techniques generates insights not delivered by one method alone. On one hand, the information from the 2D histological sections supports the interpretation of detected features within the 3D μ CT-data. On the other hand, the μ CT data can be used to determine the representative slices for histological sectioning. To this end, SR μ CT and histology are complementary methods to assess bone quality, including bony tissues formed as a result of applying augmentation materials.

More detailed research may include the morphological measurements and the histomorphometric analysis of both the three-dimensional tomography data and the series of two-dimensional slices.

The authors acknowledge the contribution of G. Schulz (University of Basel) for the helpful discussions and also like to thank S. Stübinger and B. von Rechenberg (University of Zurich) for the histological interpretation and evaluation, L. Ettinger Ferguson (University of Zurich) and her team for the assistance with histology preparation. The authors thank M. N. Holme (Imperial College London) for improving the English throughout the manuscript. Beamtime was granted through the project proposals I-20110780 EC and I-20110555 EC (HASYLAB at DESY, Hamburg, Germany).

References

- [1] D. Buser, T. von Arx, C. ten Bruggenkate, D. Weingart: *Clin. Oral Implants Res.* 11 Suppl. 1 (2000) 59. DOI:10.1034/j.1600-0501.2000.011S1059.x
- [2] J. Pietrovovski, M. Massler: *J. Prosthet. Dent.* 17 (1967) 21. DOI:10.1016/0022-3913(67)90046-7
- [3] W.L. Tan, T.L.T. Wong, M.C.M. Wong, N.P. Lang: *Clin. Oral Implants Res.* 23 (2012) 1. DOI:10.1111/clr.12011
- [4] B.S. McAllister, K. Haghishat: *J. Periodontol.* 78 (2007) 377. DOI:10.1902/jop.2007.060048
- [5] A. Horváth, N. Mardas, L.A. Mezzomo, I.G. Needleman, N. Donos: *Clin. Oral Invest.* 17 (2013) 341. DOI:10.1007/s00784-012-0758-5
- [6] D. Buser, K. Dula, D. Hess, H.P. Hirt, U.C. Belser: *Periodontol. 2000* 19 (1999) 151. DOI:10.1111/j.1600-0757.1999.tb00153.x
- [7] M.G. Araújo, J. Lindhe: *Clin. Oral Implants Res.* 20 (2009) 433. DOI:10.1111/j.1600-0501.2009.01705.x
- [8] E. Hjørtsg-Hansen: *Mund Kiefer Gesichtschir.* 6 (2002) 6. DOI:10.1007/s10006-001-0343-6
- [9] M.G. Araújo, J. Lindhe: *Clin. Oral Implants Res.* 22 (2011) 9. DOI:10.1111/j.1600-0501.2010.01937.x
- [10] S.B. Sousa, I.I. Castro-Silva, L.A.C. Da Rocha Coutinho, A. Lenharo, J.M. Granjeiro: *J. Biomim. Biomater. Tissue Eng.* 18 (2013) 85. DOI:10.4028/www.scientific.net/JBBT.18.85
- [11] C.H.F. Hämerle, R.E. Jung, A. Feloutzis: *J. Clin. Periodontol.* 29 (2002) 226. DOI:10.1034/j.1600-051X.29.s3.14.x
- [12] B. Ilgenstein, H. Deyhle, C. Jaquierey, C. Kunz, A. Stalder, S. Stübinger, G. Jundt, F. Beckmann, B. Müller, S.E. Hieber: *Proc. of SPIE* 8506 (2012) 85060 M. DOI:10.1117/12.929616
- [13] H. Sarve, J. Lindblad, C. Johansson, in: G. Bebis, R. Boyle, B. Parvin, D. Koracin, P. Remagnino, F. Porikli, J. Peters, J. Kłosowski, L. Arns, Y. Chun, T.-M. Rhyne, L. Monroe (Eds.), *Lect. Notes Comput. Sci.*, Springer Berlin Heidelberg, (2008) 1071. DOI:10.1007/978-3-540-89639-5_102
- [14] M. Seise, T. Alhonnoro, M. Kolesnik: *J. Pathol. Inform.* 2 (2011) 9. DOI:10.4103/2153-3539.92036
- [15] H. Van Campenhout, B. Van Damme, G. Van der Perre, J. Dequeker, T. Hildebrand, P. Rüegsegger: *Bone* 23 (1998) 59. DOI:10.1016/S8756-3282
- [16] G. Schulz, C. Waschkies, F. Pfeiffer, I. Zanette, T. Weitkamp, C. David, B. Müller: *Sci. Rep.* 2 (2012) 1. DOI:10.1038/srep00826
- [17] F.G. Meoli, T. Cavalieri, B. Buser, J. Smoley, L. Shen: *J. Am. Osseopath. Assoc.* 100 (2000) 703.
- [18] H.J. Johnson, G.E. Christensen: *IEEE Trans. Med. Imaging* 21 (2002) 450. DOI:10.1109/TMI.2002.1009381
- [19] D. Rueckert, L.I. Sonoda, C. Hayes, D.L. Hill, M.O. Leach, D.J. Hawkes: *IEEE Trans. Med. Imaging* 18 (1999) 712. DOI:10.1109/42.796284
- [20] F. Maes, A. Collignon, D. Vandermeulen, G. Marchal, P. Suetens: *IEEE Trans. Med. Imaging* 16 (1997) 187. DOI:10.1109/42.563664
- [21] S. Osechinskiy, F. Kruggel: *Anat. Res. Int.* 2011 (2011). DOI:10.1155/2011/287860
- [22] A. Krauth, R. Blanc, A. Poveda, D. Jeanmonod, A. Morel, G. Székely: *Neuroimage* 49 (2010) 2053. DOI:10.1016/j.neuroimage.2009.10.042
- [23] Y. Song, D. Treanor, A. Bulpitt, D. Magee: *J. Pathol. Inform.* 4 (2013) 7. DOI:10.4103/2153-3539.109864
- [24] A. Cifor, T. Pridmore, A. Pitiot: *Lec. Notes Comput. Sci.* 5636 (2009) 350. DOI:10.1007/978-3-642-02498-6_29
- [25] J. Dauguet, T. Delzescaux, F. Conde, J.-F. Mangin, N. Ayache, P. Hantraye, V. Frouin: *J. Neurosci. Meth.* 164 (2007) 191. DOI:10.1016/j.jneumeth.2007.04.017
- [26] H. Bay, T. Tuytelaars, L. Van Gool, in: *Proc. 9th Europ. Conf. Computer Vision*, Springer (2006).
- [27] G.D. Lowe: *Int. J. Comput. Vision* 60 (2004) 91. DOI:10.1023/B:VISI.0000029664.99615.94
- [28] F. Beckmann, J. Herzen, A. Haibel, B. Müller, A. Schreyer: *Proc. of SPIE* 7078 (2008) 70781D. DOI:10.1117/12.794617
- [29] S. Osswald, T. Cron, C. Gradel, P. Hilti, M. Lippert, J. Strobel, M. Schaldach, P. Buser, M. Pfisterer: *Pacing Clin. Electrophysiol.* 23 (2000) 1502. DOI:10.1046/j.1460-9592.2000.01502.x
- [30] A. Kak, M. Slaney: *Principles of computerized tomographic imaging*, IEEE Press, New York (1988).
- [31] W.N. Venables, B.D. Ripley: *Modern Applied Statistics with S*, Springer, New York (2002). DOI:10.1007/978-0-387-21706-2
- [32] D.J. Kroon, C.H. Slump, in: *IEEE Int. Symp. Biomed. Imaging*, (2009) 963. DOI:10.1109/isbi.2009.5193214
- [33] B. Müller, F. Beckmann, M. Huser, F. Maspero, G. Székely, K. Ruffieux, P. Thurner, E. Wintermantel: *Biomol. Eng.* 19 (2002) 73. DOI:10.1016/S1389-0344(02)00014-X
- [34] A. Barone, M. Ricci, P. Tonelli, S. Santini, U. Covani: *Clin. Oral Implants Res.* 24 (2013) 1231. DOI:10.1111/j.1600-0501.2012.02535.x
- [35] A. Friedmann, M. Dard, B.-M. Kleber, J.-P. Bernimoulin, D.D. Bosshardt: *Clin. Oral Implants Res.* 20 (2009) 708. DOI:10.1111/j.1600-0501.2009.01708.x
- [36] N. Mardas, V. Chadha, N. Donos: *Clin. Oral Implants Res.* 21 (2010) 688. DOI:10.1111/j.1600-0501.2010.01918.x
- [37] L. Cordaro, D.D. Bosshardt, P. Palattella, W. Rao, G. Serino, M. Chiapasco: *Clin. Oral Implants Res.* 19 (2008) 796. DOI:10.1111/j.1600-0501.2008.01565.x
- [38] F. Vignoletti, P. Matesanz, D. Rodrigo, E. Figueiro, C. Martin, M. Sanz: *Clin. Oral Implants Res.* 23 (2012) 22. DOI:10.1111/j.1600-0501.2011.02331.x
- [39] S. Kühl, C. Brochhausen, H. Götz, A. Filippi, M. Payer, B. d'Hoedt, M. Kreisler: *Clin. Oral Invest.* 17 (2013) 543.
- [40] M. Stiller, A. Rack, S. Zabler, J. Goebels, O. Dalugge, S. Jonscher, C. Knabe: *Bone* 44 (2009) 619. DOI:10.1016/j.bone.2008.10.049
- [41] A. Barone, N.N. Aldini, M. Fini, R. Giardino, J.L. Calvo Guirado, U. Covani: *J. Periodontol.* 79 (2008) 1370. DOI:10.1902/jop.2008.070628
- [42] F.C. Fierz, F. Beckmann, M. Huser, S.H. Irsen, B. Leukers, F. Witte, O. Degistrici, A. Andronache, M. Thie, B. Müller: *Biomater.* 29 (2008) 3799. DOI:10.1016/j.biomaterials.2008.06.012
- [43] L.A. Feldkamp, S.A. Goldstein, A.M. Parfitt, G. Jesion, M. Klee-rekoper: *J. Bone Miner. Res.* 4 (1989) 3. DOI:10.1002/jbmr.5650040103
- [44] R. Bernhardt, D. Scharnweber, B. Müller, P. Thurner, H. Schliephake, P. Wyss, F. Beckmann, J. Goebels, H. Worch: *Eur. Cell Mater.* 7 (2004) 42.
- [45] R. Bernhardt, E. Kuhlisch, M.C. Schulz, U. Eckelt, B. Stadlinger: *Eur. Cell Mater.* 23 (2012) 237.
- [46] E.L. Hedberg: *Tissue Eng.* 11 (2005) 1356. DOI:10.1089/ten.2005.11.1356
- [47] A. Lareida, F. Beckmann, A. Schrott-Fischer, R. Glueckert, W. Freysinger, B. Müller: *J. Microsc.* 234 (2009) 95. DOI:10.1111/j.1365-2818.2009.03143.x
- [48] G. Schulz, T. Weitkamp, I. Zanette, F. Pfeiffer, F. Beckmann, C. David, S. Rutishauser, E. Reznikova, B. Müller: *J. R. Soc. Interface* 7 (2010) 1665. DOI:10.1098/rsif.2010.0281
- [49] R. Bernhardt, J. van den Dolder, S. Bierbaum, R. Beutner, D. Scharnweber, J. Jansen, F. Beckmann, H. Worch: *Biomater.* 26 (2005) 3009. DOI:10.1016/j.biomaterials.2004.08.030
- [50] M. Dalstra, P.M. Cattaneo, F. Beckmann, M.T. Sakima, C. Lemor, M.G. Laursen, B. Melsen: *Proc. of SPIE* 6318 (2006) 631804. DOI:10.1117/12.680596
- [51] K. Patel, N. Mardas, N. Donos: *Clin. Oral Implants Res.* 24 (2013) 599. DOI:10.1111/j.1600-0501.2012.02500.x
- [52] N. Mardas, F. D'Aiuto, L. Mezzomo, M. Arzoumanidi, N. Donos: *Clin. Oral Implants Res.* 22 (2011) 416. DOI:10.1111/j.1600-0501.2010.02094.x
- [53] B. Müller, M. Riedel, P. Thurner: *Microsc. Microanal.* 12 (2006) 97. DOI:10.1017/S1431927606060168

- [54] M. Germann, A. Morel, F. Beckmann, A. Andronache, D. Jeanmonod, B. Müller: *J. Neurosci. Meth.* 170 (2008) 149.
DOI:10.1016/j.jneumeth.2008.01.011
- [55] G. Schulz, H. Crooijmans, M. Germann, K. Scheffler, M. Müller-Gerbl, B. Müller: *J. Neurosci. Meth.* 202 (2011) 17.
DOI:10.1016/j.jneumeth.2011.08.031
- [56] M.N. Holme, G. Schulz, H. Deyhle, S.E. Hieber, T. Weitkamp, F. Beckmann, J. Herzen, J.A. Lobrinus, F. Montecucco, F. Mach, A. Zumbuehl, T. Saxon, B. Müller: *Proc. of SPIE* 8506 (2012) 850609. DOI:10.1117/12.930052

(Received October 1, 2013; accepted January 20, 2014; online since February 26, 2014)

Correspondence address

Prof. Dr. Bert Müller
Biomaterials Science Center
University of Basel
c/o University Hospital
4031 Basel
Switzerland
Tel.: +41 61 265 9660
Fax: +41 61 265 9699
E-mail: bert.mueller@unibas.ch

Bibliography

DOI 10.3139/146.111050
Int. J. Mater. Res. (formerly Z. Metallkd.)
105 (2014) 7; page 679–691
© Carl Hanser Verlag GmbH & Co. KG
ISSN 1862-5282